




Research Article

Mechanical Properties of Sandstones after Freeze-Thaw Cycles and Models for Their Strength Prediction

Jiaxu Jin ¹, Junzu Ma ¹, Bing Liang,² Guosen Zhang,¹ and Shihao Yuan ¹

¹School of Civil Engineering, Liaoning Technical University, Fuxin, Liaoning 123000, China

²School of Mechanics and Engineering, Liaoning Technical University, Fuxin, Liaoning 123000, China

Correspondence should be addressed to Jiaxu Jin; jjx_605@163.com

Received 20 May 2022; Revised 14 July 2022; Accepted 23 July 2022; Published 18 August 2022

Academic Editor: Lei Weng

Copyright © 2022 Jiaxu Jin et al. This is an open access article distributed under the Creative Commons Attribution License, which permits unrestricted use, distribution, and reproduction in any medium, provided the original work is properly cited.

In cold regions, rock's load-bearing capacity will be greatly diminished in severe settings. This research investigates the influence of freezing and thawing on the physical and mechanical characteristics of sandstone, as well as the strength under complicated stress conditions. Uniaxial compression of sandstone samples was performed following freeze-thaw cycles, and the changes in elastic modulus and peak stress of dry sandstone and saturated sandstone were investigated under various freeze-thaw cycles. ANOVA was used to analyze whether there were significant differences between the number of freeze-thaw cycles and the peak strength and elastic modulus. A three-parameter strength prediction model based on σ_C , k_0 , and m is created based on the critical failure energy function. Experimental data is utilized to assess the model's correctness, and the model is used to forecast the strength of dry and saturated sandstone during freeze-thaw cycles. The result indicates that peak stress and elastic modulus of dry and saturated sandstone show a steady attenuation pattern as the number of freeze-thaw cycles increases. Brittle failure is the failure mode of dry sandstone, whereas brittle failure to plastic failure is the failure mode of saturated sandstone. After 60 freeze-thaw cycles, peak stress in dry and saturated sandstone was reduced by 55.3% and 56.8%, respectively. The three-parameter model can predict the triaxial compressive strength of specimens under different confining pressures through the uniaxial compressive strength of specimens with an error range of 1% to 13%.

1. Introduction

Rock stability in the process of tunnel excavation in cold regions has long been a hot topic. The mechanical parameters of a rock tunnel are influenced by damage within the rock [1–3]. In fact, the freeze-thaw (F-T) cycle, as well as moisture content, temperature, and other factors [4, 5] will degrade the rock, resulting in tunnel instability and accidents. In general, under natural conditions, a certain amount of moisture in the rock will improve its plastic performance [6]. However, as a result of the freezing and thawing cycles, additional cracks will result in damage [7]. The growth of interior fissures becomes more perfect as the freezing and thawing times rise, and the bonding force between particles is increasingly weakened by hydration and frost heaving force, diminishing the bearing capacity of rock. F-T action will have a direct impact on tunnel engineering safety [8–10]. As a result, significant research topics in tunnel engineering

are the mechanical properties of rock under the operation of the F-T cycle.

When the water in the pores of the rock turns from liquid to solid, the volume expands by 9%, and the constant migration of water molecules causes the rock damage to worsen, which may cause slope instability [11–14]. Fan [15] investigated the features of stress variations over time in a F-T cycle sandstone loading experiment. Based on the combined action of F-T and load, Zhou et al. [16] looked at the sandstone from a microscopic perspective. The porosity rose as the F-T periods increased, and a link between porosity and peak strength was discovered. Gasc Barbier et al. [17] analyzed the crack propagation of rock mass after F-T cycles from the perspective of elastic waves. Zhang et al. [18] found a link between the number of F-T cycles and rock tensile strength (UTS) and anisotropy and discovered that as the number of F-T cycles increased, so did the anisotropy of rock tensile strength. Zhang et al. [19] developed a damage

equation based on several types of damage and discovered that increasing the initial load reduces the damage produced by F-T. Jihwan Park et al. [20] investigated the impact of F-T cycles on internal rock structural alterations. Water caused interior particles to loosen and new cracks as a result of volume expansion. They concluded that F-T damage had less of an impact on the deterioration of granite with thick pores. Ke et al. [21] carried out different times of F-T cycles on sandstone to study the characteristics of internal pore development. The pores changed from small pores to medium pores and large pores, and the connectivity of pores led to the decrease of peak stress. Huang et al. [22] monitored the pore structure changes of sandstone under F-T by MIP (mercury intrusion porosimetry). Nanopores and micropores had gradually developed into macropores with F-T. The results showed that, with the increase of F-T cycles, the cohesion of sandstone decreased and the internal friction angle increased. Liu et al. [23] used the improved fatigue damage model to study the F-T degradation mechanism of clay-bearing sandstone under unsaturated state and predicted the strength of clay-bearing red sandstone under different F-T cycles. Kahraman and Ozdemir [24] used four different machine-learning techniques to predict the uniaxial compressive strength (USC), specific gravity (SG), water absorption rate (WA), Los Angeles abrasion (LA), P-wave velocity (Vp), and freeze-thaw resistance (F-T) tests. The results showed that machine-learning could be successfully used to predict F-T resistance. Liu et al. [25] took F-T damage into account and used P-wave velocity to replace other parameters of rock to establish a model to predict UCS of rock with different F-T cycles. However, P-wave velocity cannot precisely forecast the strength of rock because of the anisotropy in the rock. Although the existing research results have analyzed the influence of F-T cycle on rock physical and mechanical parameters in detail, the effect of F-T on each physical and mechanical parameters of sandstone is different. Some scholars only study the influence of F-T cycle on a single physical and mechanical property. They do not further analyze which factors were more sensitive to F-T. In fact, it is very important to find out which mechanical parameters are more sensitive to the F-T cycle so as to take some measures to increase the stability of rock. The strength prediction model based on the mechanical parameters obtained by the uniaxial compression experiment can decrease the strength prediction error caused by rock anisotropy.

In this paper, combined with the effect of F-T on the physical and mechanical properties of sandstone, the peak strength and elastic modulus of sandstone with different F-T cycles were tested, and the variance analysis method (ANOVA) in statistics was used to quantitatively analyze the influence of F-T factors on the peak strength and elastic modulus. Based on the critical failure energy function, the compressive strength of sandstone under complex stress is reasonably predicted.

2. Materials and Methods

2.1. Preparation of Sandstone Samples. The rock samples in this experiment were taken from the same intact rock block

without joints, and 20 sandstone samples of $\Phi 50 \text{ mm} \times 100 \text{ mm}$ were prepared according to the standards of the International Society of Rock Mechanics. During cutting, the unevenness of the upper and lower ends of the rock sample was not more than 0.05 mm, and the height error of each rock sample was within 0.3 mm. Ultrasonic velocity test was carried out on the samples with complete appearance, and 20 samples with similar quality were selected and divided into 10 groups (2 samples in each group). The first five groups were dried in the oven to remove the excessive moisture in the sample, and the latter five groups were treated with vacuum saturation method to make the sample fully saturated. The preparation of dry and saturated samples is shown in Figure 1.

Firstly, 20 cut samples were put into the oven and dried at a constant temperature of 105° for 48 h. Ten remaining samples were put into the vacuum water saturation device and stored for 48 hours to prepare the saturated samples. The air pressure in the device was controlled at -0.1 MPa during the whole process. The saturated moisture content of the sample is about 3.1%.

The obtained dry and saturated samples were subjected to 5, 10, 20, 40, and 60 F-T cycles at -20°C and 20°C . The sample numbers are shown in Table 1, and the process is shown in Figure 2.

2.2. Test Method and Process. In this experiment, TAW-2000 electrohydraulic servo rock triaxial test instrument was used for uniaxial compression test. The maximum test force of the instrument was 2000 kN. The load and axial deformation of the sample during compression were directly measured by the instrument display system. In the process of uniaxial compression, in order to obtain the full stress-strain curve of the specimen, displacement was controlled at the rate of 0.05 mm/min when loading [26].

3. Results and Discussion

3.1. Physical and Mechanical Properties of Samples after F-T Cycles

3.1.1. Variation of Stress-Strain Curves of Sandstone Samples. Based on the uniaxial compression test after F-T cycles, the stress-strain curves of dry and saturated sandstone after 5, 10, 20, 40, and 60 F-T cycles are recorded as shown in Figure 3.

With the increase of F-T cycles, the peak stress of sandstone decreases gradually. The peak stress of dry sandstone decreases obviously by 11.13 MPa after 40 F-T cycles. The peak stress of saturated sandstone decreased by 13.83 MPa after 10 F-T cycles. After 5 F-T cycles, the peak strength of dry rock samples decreases by 55.3% and that of saturated rock samples decreases by 56.8% after 60 F-T cycles.

In the early stage of loading process, the sandstone is in the pore compaction stage, and the curve is characterized by concave growth. As the skeleton of the pore compacted sandstone begins to bear the load and the force is within the elastic range, the stress-strain curve is nearly a straight line.

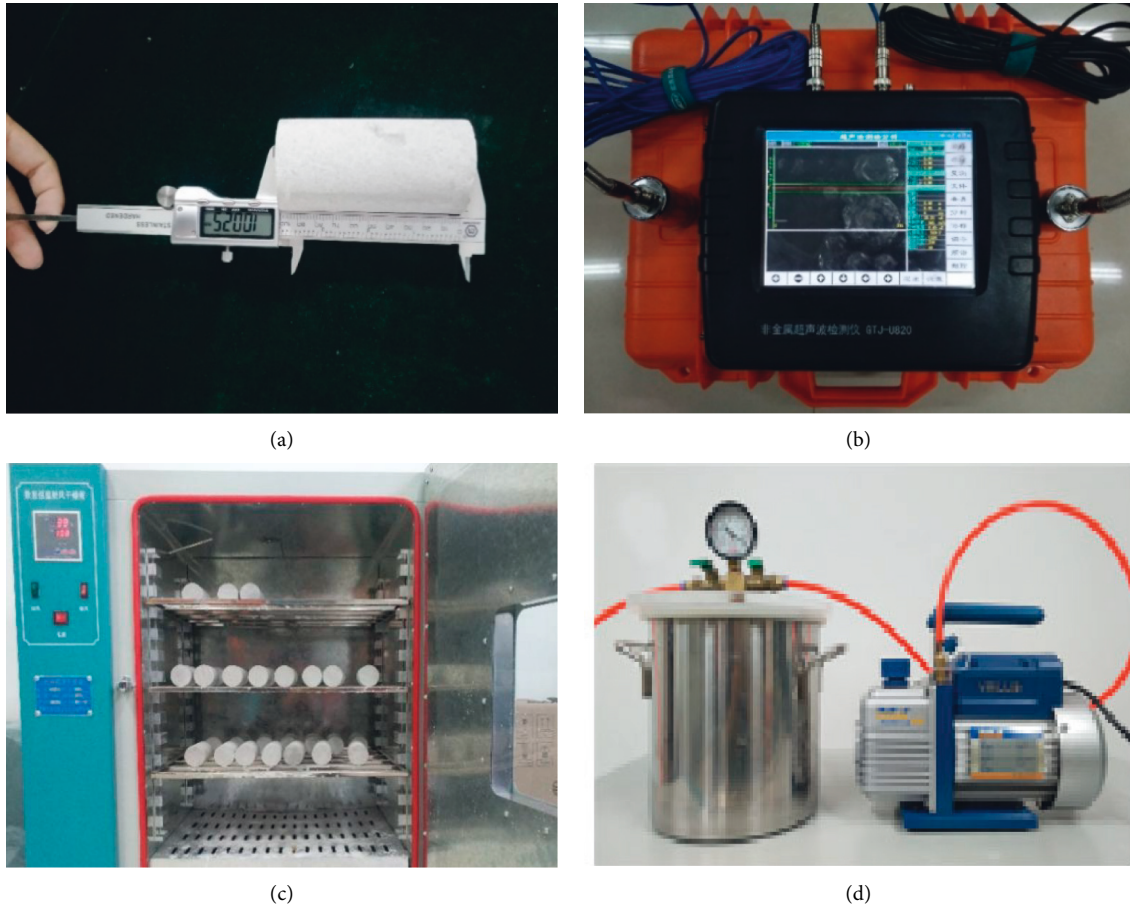


FIGURE 1: Selection and preparation of samples. (a) Smoothness test. (b) Wave speed measurement. (c) Dryer drying. (d) Vacuum saturation device.

TABLE 1: Test specimen number.

		Experimental method		Number
F-T cycle test	State dry	Freezing and thawing times		
		5	IA	
		10	IB	
		20	IC	
		40	ID	
		60	IE	
	Saturate	5	IIA	
		10	IIB	
		20	IIC	
		40	IID	
		60	IIE	

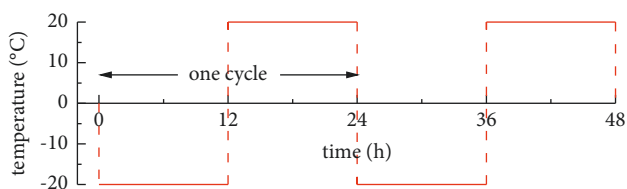


FIGURE 2: F-T cycle test.

When it reaches the yield stress, the sandstone particles produce vertical slip, and the internal microcracks gradually grow and plastic deformation occurs. When the stress reaches the peak value, the microcracks generated in the yield stage are connected to each other to form a fracture surface. At this point, the strain continues to increase, and the instantaneous decrease of stress indicates the failure of sandstone.

3.1.2. Effect of F-T Cycles on Peak Stress and Elastic Modulus of Sandstone with Different Water Content. With the increase of F-T cycles, the stress-strain slopes of all samples gradually slow down. Under the action of freezing and thawing, the thermal expansion and contraction of the cementing material in the dry sandstone lead to the continuous change of pore volume and the gradual decrease of the maximum tension. With the increase of F-T cycles, the pores in the sandstone gradually lose elasticity, resulting in the decrease of the peak strength and elastic modulus of the sandstone. For saturated sandstones containing internal water, freezing and thawing under the action of water-ice phase change result in greater pore volume expansion. The presence of water also impairs the interaction force of internal particles and the degree of compactness, resulting in loss of sandstone peak strength. Since the

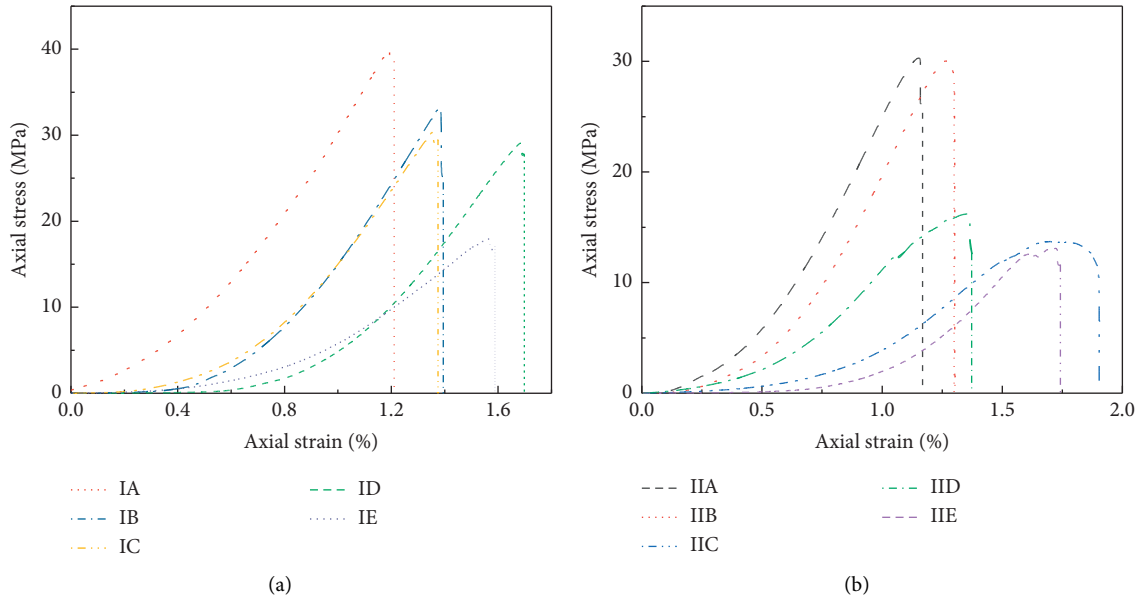


FIGURE 3: Stress-strain relationship of sandstone with different F-T cycles. (a) Dry sandstone. (b) Saturated sandstone.

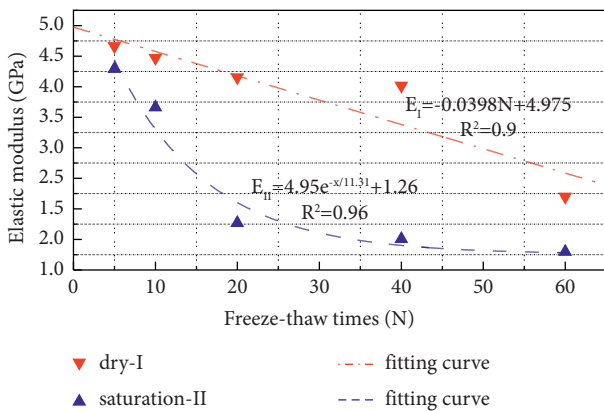


FIGURE 4: Fitting curve of elastic modulus of sandstone with different moisture contents with F-T cycles.

water content of saturated sandstone is higher than that of dry sandstone, and the volumetric deformation produced in the freezing process is greater than that of dry sandstone, therefore, the bearing capacity of dry sandstone will change significantly only after considerable F-T cycles while the saturated sandstone is sensitive to F-T action and the peak stress decreases quickly even after several cycles. After 60 F-T cycles, the peak stress of saturated sandstone is 1.5% higher than that of dry sandstone.

The elastic modulus of sandstone changes as shown in Figure 4.

As the number of F-T cycles increases, the elastic modulus of dry sandstone decreases linearly while that of saturated sandstone decreases exponentially. The elastic modulus of dry sandstone decreases by 52.8% and that of saturated sandstone decreases by 69.7% after 60 F-T cycles.

With the increase of F-T cycles, the internal structure of dry sandstone changes almost uniformly, and the evolution rate of pore throat is close to uniform, which

leads to a certain linear relationship between macroscopic mechanical properties and F-T cycles. In the saturated sandstone, due to the existence of pore water, the pore development is random under the action of F-T. In the initial cycles, the pores in the saturated sandstone expand sharply and thus the elastic modulus decreases rapidly. However, with the internal pores connected, the elastic modulus of the sandstone gradually tends to be stable, and no large cracks but only some small cracks will be produced. Hence, the elastic modulus of the sandstone decreases slowly. Since the water content of saturated sandstone is higher than that of dry sandstone, the internal damage is more severe, and the elastic modulus of saturated sandstone is 6.9% lower than that of dry sandstone after 60 F-T cycles.

3.1.3. Statistical Analysis. The statistical methods for analysis are designed to determine whether moisture content has a significant effect on sandstone peak strength and elastic modulus. This section delves into the details of the issue. Because the average value of the drop in peak strength and elastic modulus after 60 F-T cycles follows the normal distribution in statistics, the number of F-T cycles is used to group the samples and determine whether there are significant variations between groups.

An analysis of variance (ANOVA) was conducted to investigate if there were statistically significant differences in peak strength and elastic modulus between sandstone sample groups with different F-T cycles. When using single factor analysis of variance to study sandstone samples with 100% saturation, there is always a control group for comparison.

The original hypothesis in this experiment is that there is no significant difference in the average μ between groups, indicating that $\mu_1 = \mu_2 = \mu_3$. Assuming that the explicitness

TABLE 2: Results of peak strength and elastic modulus.

Group		Degree of saturation = 100%					
		Sample 1	Sample 2	Sample 3	Mean	SD ^a	COV ^b
F-T times-peak strength	5	30.35	32.68	33.56	32.20	1.66	5.2
	10	30.04	32.13	33.26	31.81	1.63	5.1
	20	16.23	17.35	19.23	17.60	1.52	8.6
	40	13.75	14.25	16.32	14.77	1.36	9.2
	60	13.15	14.81	15.26	14.41	1.11	7.7
F-T times-elastic modulus	5	4.29	4.56	4.73	4.53	0.22	4.9
	10	3.66	3.75	3.8	3.74	0.07	1.9
	20	1.77	1.82	2.13	1.91	0.20	10.5
	40	1.53	1.79	1.94	1.75	0.21	12
	60	1.3	1.45	1.51	1.42	0.11	7.7

^aStandard deviation and ^bcoefficient of variation.

TABLE 3: Summary of statistical analysis.

	ANOVA calculations					
	R	N	SSE	SSA	F	F _{α=0.05}
F-T times-peak strength	5	15	21.62	987.89	114.23	3.48
F-T times-elastic modulus	5	15	0.294	22.71	193.08	3.48

level $\alpha = 0.05$, the total amount of samples is defined as N , N is divided into r different groups according to different moisture contents, for instance, sandstone samples with five F-T cycles consider three different moisture contents of 0, 2.262%, and 3.77%, each moisture content group contains 10 samples, r is equal to 10, and N is equal to 30.

In the process, the following procedure must be followed [27].

$$SSE = \sum_{R=1}^k \sum_{m=1}^{N_k} (x_{mR} - \bar{x}_R)^2, SSA = \sum_{R=1}^k \sum_{m=1}^{N_k} (\bar{x}_R - \bar{x})^2 \bar{x} = \frac{1}{N} \sum_{R=1}^k \sum_{m=1}^{N_k} X_{mR}. \quad (1)$$

According to F statistics,

$$F = \frac{SSA / (k - 1)}{SSE / (N - R)}, \quad (2)$$

where N is the total number of sandstone samples; R refers to groups by number of F-T cycles; \bar{x} is the average value of each group; SSE is the intragroup variation; SSA is the intergroup variation.

Thus, if $F \leq F_{\alpha=0.05}$, the original assumption will not be rejected; then, $\mu_1 = \mu_2 = \mu_3$, which indicates that the differences between the means are statistically insignificant.

If $F > F_{\alpha=0.05}$, the hypothesis is rejected, then $\mu_1 = \mu_2 = \mu_3$, and thus the means are significantly different. Table 2 summarizes the results of peak strength and elastic film of saturated sandstone samples with five different F-T cycles. Table 3 presents a summary of the statistical analysis.

3.2. Critical Failure Energy Function. The M-C strength criterion establishes the mathematical relationship between shear stress τ and normal stress σ through the envelope of

the limit Mohr circle and accurately describes the ultimate stress state of each point of the fracture surface to a certain extent. Assuming that the friction coefficient between the fracture surfaces is constant, the limit equilibrium state of sliding friction just meets the M-C strength criterion. When rock mass is subjected to force, longitudinal and lateral deformations are generated macroscopically. These two kinds of deformations lead to the destruction of rock mass, namely, shear failure of rock mass and expansion failure of rock mass. According to the functional principle, when the rock mass is unstable, the critical failure energy required for two forms of deformation on the fracture surface is provided by the shear stress and normal stress at this point. The potential energy stored by the shear stress τ_p in the fracture surface under elastic shear strain γ_p as well as the potential energy stored by the normal stress σ_p under volumetric strain ε_v can be expressed as follows [28]:

$$e = \frac{\tau_p \gamma_p}{2 - \sigma_p \varepsilon_v} = \frac{\tau_p^2}{(2\mu)} - \frac{\sigma_p \sigma_v}{(3K)}, \quad (3)$$

where e is the strain energy when the unit breaks; μ and K represent the shear elastic modulus and bulk modulus when the material is damaged; σ_v is volume stress: $\sigma_v = \sigma_1 + \sigma_2 + \sigma_3$. When loading, the positive stress σ_v prevents the formation of rock fracture, so it provides negative energy.

In three-dimensional principal stress space, $(\sigma_1, \sigma_2, \sigma_3)$ is designated as maximum principal stress, intermediate principal stress, and minimum principal stress, respectively. Assuming that the direction of the crack plane is (l, m, n) , the shear stress τ_p and the normal stress σ_p can be expressed as

$$\sigma_p = l^2 \sigma_1 + m^2 \sigma_2 + n^2 \sigma_3, \quad (4)$$

$$\tau_p^2 = l^2 \sigma_1^2 + m^2 \sigma_2^2 + n^2 \sigma_3^2 - \sigma_p^2. \quad (5)$$

According to the criterion of geometric space vector,

$$l^2 + m^2 + n^2 = 1. \quad (6)$$

Formulas (4)–(6) are substituted into equation (3) to obtain

$$e = \left(\frac{1}{2\mu}\right) \left\{ [(\sigma_1 + \sigma_3)^2(l^2 + l^4) + (\sigma_2 + \sigma_3)^2(m^2 + m^4) - 2(\sigma_1 - \sigma_3)(\sigma_2 - \sigma_3)l^2m^2] - 2k\sigma [(\sigma_1 - \sigma_3)l^2 + (\sigma_2 - \sigma_3)m^2 + \sigma_3] \right\}. \quad (7)$$

The parameter k is defined as

$$k = \frac{\mu}{3K}. \quad (8)$$

When the rock is unstable, the energy e reaches the peak value and cracks are produced. Through $\partial e/\partial l$, $\partial e/\partial m$, the cracking direction under the critical energy state is solved:

$$l^2 = \left(\frac{1}{2}\right) \left[\frac{1 - 2k\sigma_v}{(\sigma_1 - \sigma_3)} \right] m^2 = 0. \quad (9)$$

Substituting equation (9) into (7), the failure energy e_d under the critical strain at one point of the fracture surface is

$$e_d = (8\mu)^{-1} [(\sigma_1 - \sigma_3)^2 - 4k\sigma_v(\sigma_1 + \sigma_3) + 4k^2\sigma_v^2]. \quad (10)$$

When the rock mass is destroyed, the failure energy e_d acts on both sides of the crack in the form of surface energy. According to the law of conservation of energy, it is known that

$$e_d = (8\mu)^{-1} [(\sigma_1 - \sigma_3)^2 - 4k\sigma_v(\sigma_1 + \sigma_3) + 4k^2\sigma_v^2] = 2\gamma_s, \quad (11)$$

where γ_s is the unit surface energy of the fracture surface, and the sum of surface energy on both sides of the fracture is $2\gamma_s$. When pure shear failure occurs on the rock $\sigma_v = 0$, equation (11) can be simplified as

$$(\sigma_1 - \sigma_3)^2 (8\mu)^{-1} = \tau_0^2 (2\mu)^{-1} = 2\gamma_s, \quad (12)$$

where τ_0 is the shear strength of rock. After substituting formulas (12) into (11), we get

$$(\sigma_1 - \sigma_3)^2 - 4k\sigma_v(\sigma_1 + \sigma_3) + 4k^2\sigma_v^2 = 4\tau_0^2. \quad (13)$$

Formula (13) describes the critical failure stress state of rock based on the M-C criterion model. When the rock sample is under uniaxial compression, the parameter $k = k_0$, according to formula (13):

$$\sigma_C = 2\tau_0(1 - 2k_0), \quad (14)$$

where σ_C represents UCS. Using σ_C to denote the offspring of τ_0 into equation (15), we get

$$\left[\frac{(\sigma_1 - \sigma_3)}{\sigma_C} \right]^2 - 4k \left(\frac{\sigma_v}{\sigma_C} \right) \left[\frac{(\sigma_1 + \sigma_3)}{\sigma_C} \right] + 4k^2 \left(\frac{\sigma_v}{\sigma_C} \right)^2 = (1 - 2k_0)^2, \quad (15)$$

where $k_0 = 0.5(1 - 2\varepsilon\nu)/(1 + \varepsilon\nu)$ and ε represents a reduction factor for Poisson's ratio at failure. It represents the condition of critical failure energy when σ_C is reached.

When the rock is subjected to triaxial compression, the volume expansion will occur before failure, and the volume deformation of rock is nonlinear. The deformation relationship between rock volume expansion and failure is expressed by power function:

$$\varepsilon_V = A\sigma_V^m, \quad (16)$$

where A represents the empirical constant related to rock properties and σ_E represents the stress in volume expansion of rock: $\varepsilon m \approx \sigma_E/\sigma_C$.

If equation (16) represents the linear relationship between volumetric stress and volumetric strain with respect to volumetric modulus K ,

$$K = \frac{\sigma_V^{1-m}}{(3A)}. \quad (17)$$

From formulas (8), (16), and (17),

$$k = A\mu\sigma_V^{m-1}. \quad (18)$$

In uniaxial compression $\sigma_V = \sigma_C k = k_0$, the substitution of equation (18) can be obtained:

$$k = k_0 \left(\frac{\sigma_C}{\sigma_V} \right)^{1-m}. \quad (19)$$

Formula (19) can be replaced by formula (15):

$$\left[\frac{(\sigma_1 - \sigma_3)}{\sigma_C} \right]^2 - 4k_0 \left(\frac{\sigma_v}{\sigma_C} \right)^m \frac{(\sigma_1 + \sigma_3)}{\sigma_C} + 4k_0^2 \left(\frac{\sigma_v}{\sigma_C} \right)^{2m} = (1 - 2k_0)^2. \quad (20)$$

Formula (20) can be used to predict the strength of specimens under different confining pressures by determining the three parameters of σ_C , k_0 , m . It is a theoretical model of the power function relationship of the rock volumetric strain approximate to formula (16) when the failure occurs.

3.2.1. Model Verification. The uniaxial stress test is used to predict the compressive strength of rock under complex stress state, which is a convenient method for construction in practice. The following analysis is based on the research results published by scholars [29] to validate the accuracy of the theory.

Table 4 shows the physical and mechanical parameters obtained by uniaxial compression test on granite rock. The theoretical predicted strength values of granite under complex stress state can be obtained by the calculation formulas of k_0 and m and the experimental data in Table 3. As the granite belongs to type II characteristic rock, Poisson's ratio reduction factor ξ of 0.2 is taken to calculate k_0 . The strength prediction results are shown in Figure 5. Through comparison, it can be found that the theoretical value of strength slows down with the increase of confining pressure. The predicted value of theoretical strength is slightly higher than the actual strength value,

TABLE 4: The uniaxial compression test results and material parameters of granite.

Sample number	Compressive strength σ_c /MPa	Poisson ratio ν	Starting point of expansion σ_E /MPa	Parameter k_0	Parameter m
1	173.5	0.27	142.9	0.423	0.823
2	72.9	0.25	49.0	0.428	0.671
3	66.7	0.29	50.8	0.418	0.762
4	121.7	0.37	94.7	0.396	0.778
5	68.6	0.31	50.0	0.412	0.730
6	129.8	0.31	98.5	0.412	0.760
7	75.4	0.22	55.4	0.438	0.735
8	100.8	0.26	78.8	0.425	0.782
9	93.9	0.28	70.5	0.419	0.750
10	75.43	0.23	52.5	0.434	0.700
11	83.9	0.25	60.3	0.428	0.719
12	106.4	0.22	74.7	0.438	0.702
13	105.6	0.29	79.6	0.417	0.753
14	81.5	0.23	65.9	0.434	0.808

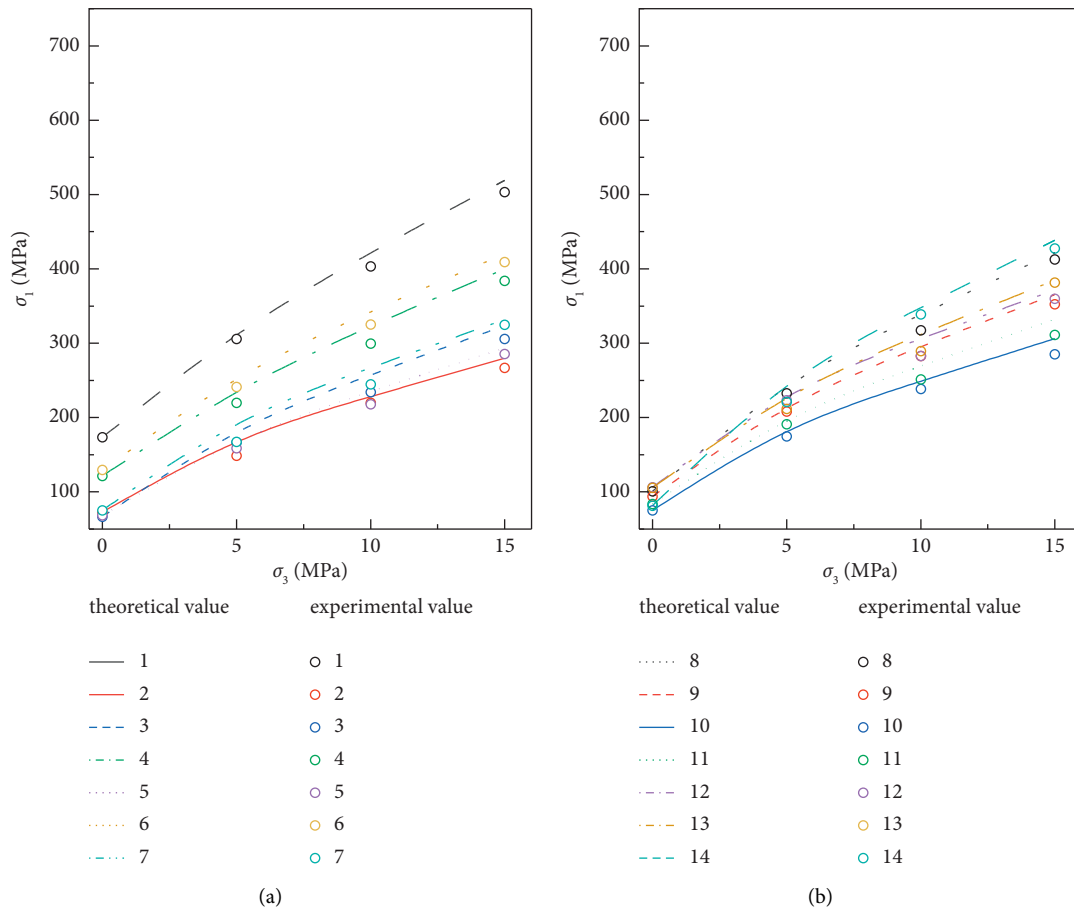


FIGURE 5: Comparison of theoretical and actual strength of granite.

with the error of 1%–13%, indicating that the established prediction model of this theory can approximately predict the rock strength under complex stress state.

3.2.2. *Strength Prediction.* Based on the model established by the critical failure energy function, the strengths of sandstone under complex stress state after F-T cycles are

predicted. The experimental results and material parameters of these sandstones are shown in Table 5.

The predicted strength of sand under complex stress state can be obtained by substituting the calculation formula of the parameters k_0 and m of each sandstone and the experimental data shown in the table into equation (20). Since the stress-strain curve of sandstone belongs to type I, the

TABLE 5: Uniaxial compression test results and material parameters of F-T sandstone.

Sample number	Compressive strength σ_c /MPa	Poisson ratio ν	Starting point of expansion σ_E /MPa	Parameter k_0	Parameter m
IA	40.1	0.212	19.2	0.423	0.823
IB	33.3	0.211	15.1	0.428	0.671
IC	30.5	0.238	14.3	0.418	0.762
ID	29.1	0.241	14.4	0.396	0.778
IE	18.0	0.242	8.13	0.412	0.730
IIA	30.3	0.237	13.7	0.412	0.760
IIB	30.0	0.238	13.4	0.438	0.735
IIC	16.2	0.243	7.3	0.425	0.782
IID	13.7	0.246	6.2	0.419	0.750
IIE	13.1	0.245	5.9	0.434	0.700

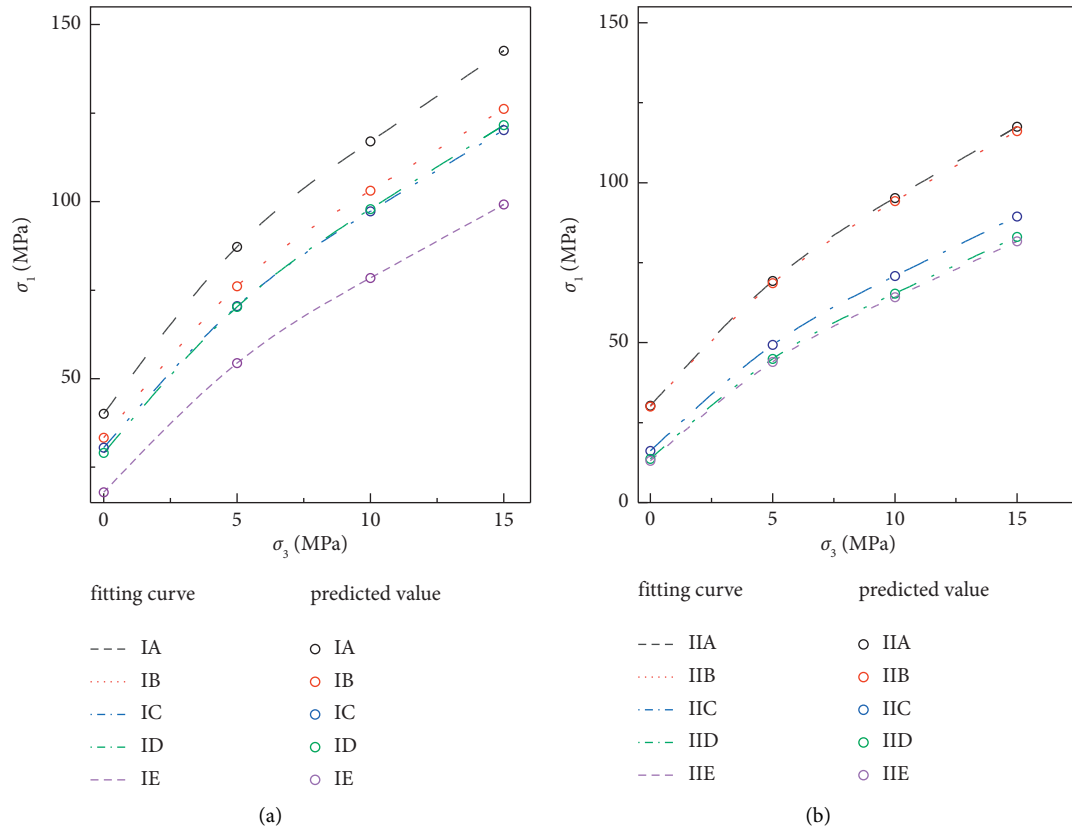


FIGURE 6: Fitting curve of theoretical strength of F-T sandstone with different moisture contents.

reduction coefficient of Poisson ratio is 1/3 when calculating k_0 and the strength prediction results are shown in Figure 6. σ_1 of dry sandstone (Figure 6(a)) and saturated sandstone (Figure 6(b)) increases with the increase of σ_3 , and the increase rate of σ_1 is rapid at first but slows down with the increase of σ_3 . When σ_3 increases to a certain extent, the growth rate of predicted strength of sandstone tends to be flat. The model can well predict the ultimate strength of rocks in cold regions after F-T cycles.

3.3. Discussion. The UCS and elastic modulus of sandstone samples decrease to varying degrees after F-T cycles. The average peak strength decreases from 32.20 MPa to

14.41 MPa, and the average elastic modulus decreases from 4.53 GPa to 1.42 GPa. The F values of peak strength and elastic modulus calculated by ANOVA are 114.23 and 193.08, respectively, which are much larger than 3.48, indicating that F-T cycles can significantly affect the mechanical properties of sandstone, and the elastic modulus is more sensitive to F-T cycles. H. Yavuz et al. analyzed the effect of F-T cycle on peak strength and P-wave velocity by multiple regression analysis. They believed that the effect of F-T cycle on peak strength was more obvious [30], which was consistent with the conclusions of many scholars [31]. The results of Liu's research showed that with the increase of confining

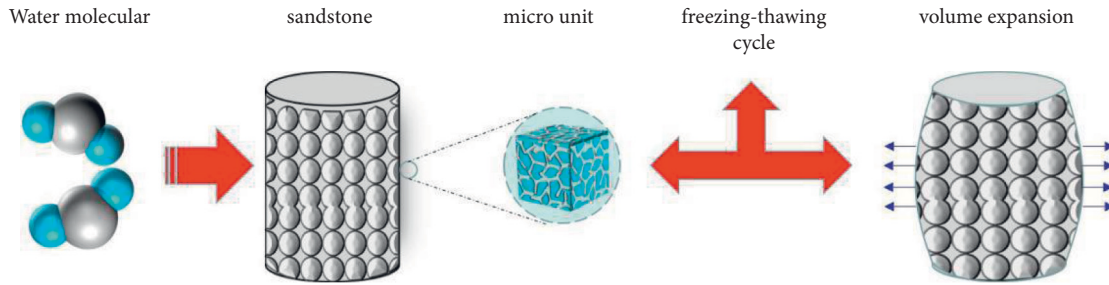


FIGURE 7: Mechanism of freezing and thawing damage.

pressure, the peak stress of coal rock increased, and the ductility of coal rock became more obvious [32], which further verifies the prediction results of the three-parameter model.

4. Conclusions

In this paper, five distinct F-T cycles were performed on two different types of sandstone with variable water content. The stress-strain curve was obtained by uniaxial compression of the specimen with variations in F-T cycles and water content. The relationship between elastic modulus, peak strength, and F-T times was investigated. The apparent differences between five distinct F-T cycles of saturated sandstone were compared using analysis of variance (ANOVA). Finally, the energy failure critical function was used to estimate the specimen's strength under complex stress conditions, resulting in a strength prediction model.

- (1) Peak strength and elastic modulus are reduced as a result of the F-T cycle. Cementing force decreases as the physical properties of internal cementing materials change owing to F-T cycles. The internal water-ice phase transition causes the volume of the saturated sandstone to vary, and the frost heaving force between the particles causes the physical and mechanical properties of the entire sample to change.
- (2) The freezing-thawing cycle can drastically impair the peak strength and elastic modulus of sandstone samples, according to the results of variance analysis (ANOVA). Due to the filling of small pores by water molecules, water molecules migrate during the melting process, and new small cracks are generated between particles during the freezing process. Finally, the pores are joined to produce huge cracks, resulting in macroscale volume expansion as illustrated in Figure 7, which has a major impact on the samples' peak strength and elastic modulus.
- (3) A three-parameter strength prediction model based on σ_c , k_0 , and m is created based on the critical failure energy theory, assuming that the shear modulus of elasticity is constant and the pressure of bulk modulus changes exponentially. According to experimental results reported by various scholars, the model's error ranges from 1% to 13%. When

using this model to forecast the strength of sandstone samples under complicated stress circumstances, the sample's σ_1 increases with the increase of σ_3 . The sandstone samples with more F-T cycles and saturated water rise more slowly, although their curves are generally flat.

Data Availability

The data used to support the findings of this study are included within the article.

Conflicts of Interest

The authors declare that there are no conflicts of interest.

Acknowledgments

The authors appreciate the National Natural Science Fund and the Liaoning Provincial Department of Education's financial assistance for scientific research endeavors. This work was funded by the National Natural Science Foundation of China (51974145 and 51904144) and the Scientific Research Funding Project of Liaoning Provincial Department of Education (LJKZ0354).

References

- [1] C. J. A. S. Deangeli, "Failure in the tension zone around a circular tunnel excavated in saturated porous rock," *Applied Sciences*, vol. 11, no. 18, pp. 8384–84, 2021.
- [2] J. Ding, Y. Wang, and A. Dong, "Study on structural health and safety evaluation of in-service municipal tunnels," *Sichuan Building Materials*, vol. 48, no. 1, pp. 224–225, 2022.
- [3] H. Cui, J. Ji, J. Song, and W. Huang, "Limit state line-based seismic stability charts for homogeneous earth slopes," *Computers and Geotechnics*, vol. 146, p. 104749, 2022.
- [4] L. Meng, L. Han, H. Zhu, W. Dong, and W. Li, "Influence of moisture content on the structural characteristics of argillaceous weakly consolidated rock caused by dynamic loading in the coal mine," *Shock and Vibration*, vol. 2021, pp. 1–18, Article ID 7206801, 2021.
- [5] G. G. Tsyphkin, "On stability of a water injection front in high temperature rock," *Fluid Dynamics*, vol. 56, no. 6, pp. 828–835, 2021.
- [6] P. Wang, T. Li, and J. Hua, "Experimental study on impact tendency of sandstone under different water contents," *Shanxi Coal*, vol. 39, no. 5, pp. 30–34, 2020.

- [7] A. Momeni, Y. Abdilor, G. R. Khanlari, M. Heidari, and A. A. Sepahi, "The effect of freeze-thaw cycles on physical and mechanical properties of granitoid hard rocks," *Bulletin of Engineering Geology and the Environment*, vol. 75, no. 4, pp. 1649–1656, 2016.
- [8] Z. Li, Y. Cui, and J. Jia, "Long-term stability of tunnels in cold regions under freeze-thaw cycles," *Science Technology and Engineering*, vol. 22, no. 5, pp. 2032–2039, 2022.
- [9] P. Xu, Y. Wu, L. Huang, and K. Zhang, "Study on the progressive deterioration of tunnel lining structures in cold regions experiencing freeze-thaw cycles," *Applied Sciences*, vol. 11, no. 13, p. 5903, 2021.
- [10] Q. Guo, H. Su, and H. Jing, "Effect of wetting-drying cycle on the deformation and seepage behaviors of rock masses around a tunnel," vol. 2020, pp. 2020–14.
- [11] C. Xia, Y. Wang, and J. Zheng, "Study on uneven frost heaving of fractured rock mass," *Rock and Soil Mechanics*, vol. 41, no. 4, pp. 1161–1168, 2021.
- [12] Y. Hong, Z. Shao, G. Shi, Y. Dou, W. Wang, and W. Zhang, "Freeze-thaw effects on stability of open pit slope in high-altitude and cold regions," *Geofluids*, vol. 2021, pp. 1–10, Article ID 8409621, 2021.
- [13] Y. Li, C. Ma, L. Zhang, and B. Li, "Influence research for softening and swelling of weakly cemented soft rock on the stability of surrounding rock in roadway," *Geofluids*, vol. 2022, pp. 1–12, 2022.
- [14] J. Jin, Z. Qin, X. Lü et al., "Rheology control of self-consolidating cement-tailings grout for the feasible use in coal gangue-filled backfill," *Construction and Building Materials*, vol. 316, p. 125836, 2022.
- [15] Q. Fan, "Study on mechanical properties of dam foundation rock mass under the influence of freeze-thaw cycle," *Technical Supervision in Water Resources*, vol. 2022, no. 3, pp. 120–121+147, 2022.
- [16] K. p. Zhou, B. Li, J. l. Li, Hw. Deng, and F. Bin, "Microscopic damage and dynamic mechanical properties of rock under freeze-thaw environment," *Transactions of Nonferrous Metals Society of China*, vol. 25, no. 4, pp. 1254–1261, 2015.
- [17] M. Gasc-Barbier and V. J. G. Merrien-Soukatchoff, "Effect of freezing-thawing cycles on the elastic waves' properties of rocks," vol. 12, no. 3, p. 103, 2022.
- [18] J. Zhang, H. Fu, Z. Huang, Y. Wu, W. Chen, and Y. Shi, "Experimental study on the tensile strength and failure characteristics of transversely isotropic rocks after freeze-thaw cycles," *Cold Regions Science and Technology*, vol. 163, pp. 68–77, 2019.
- [19] H. Zhang, X. Meng, and X. Liu, "Establishment of constitutive model and analysis of damage characteristics of frozen-thawed rock under load," *Arabian Journal of Geosciences*, vol. 14, no. 13, p. 1277, 2021.
- [20] J. Park, C.-U. Hyun, and H.-D. Park, "Changes in micro-structure and physical properties of rocks caused by artificial freeze-thaw action," *Bulletin of Engineering Geology and the Environment*, vol. 74, no. 2, pp. 555–565, 2014.
- [21] B. Ke, K. Zhou, H. Deng, and F. Bin, "NMR pore structure and dynamic characteristics of sandstone caused by ambient freeze-thaw action," *Shock and Vibration*, vol. 2017, pp. 1–10, 2017.
- [22] S. B. Huang, S. L. Yu, Y. H. Ye, Z. Ye, and A. Cheng, "Pore structure change and physico-mechanical properties deterioration of sandstone suffering freeze-thaw actions," *Construction and Building Materials*, vol. 330, p. 127200, 2022.
- [23] Y. Liu, Y. Cai, S. Huang, Y. Guo, and G. Liu, "Effect of water saturation on uniaxial compressive strength and damage degree of clay-bearing sandstone under freeze-thaw," *Bulletin of Engineering Geology and the Environment*, vol. 79, no. 4, pp. 2021–2036, 2019.
- [24] E. Kahraman and A. C. Ozdemir, "The prediction of durability to freeze-thaw of limestone aggregates using machine-learning techniques," *Construction and Building Materials*, vol. 324, p. 126678.
- [25] Q. Liu, S. Huang, Y. Kang, and X. Liu, "A prediction model for uniaxial compressive strength of deteriorated rocks due to freeze-thaw," *Cold Regions Science and Technology*, vol. 120, pp. 96–107, 2015.
- [26] X. D. Zhao, H. X. Zhang, and W. C. Zhu, "Fracture evolution around pre-existing cylindrical cavities in brittle rocks under uniaxial compression," *Transactions of Nonferrous Metals Society of China*, vol. 24, no. 3, pp. 806–815, 2014.
- [27] R. G. Shaw and T. J. E. Mitchell-Olds, "ANOVA for unbalanced data: an overview," *Ecology*, vol. 74, no. 6, pp. 1638–1645, 1993.
- [28] D. Lin, J. Du, and H. Liu, "Energy description of Mohr-Coulomb criterion model," *Journal of North China Institute of Science and Technology*, vol. 17, no. 2, p. 9, 2020.
- [29] Y. Wang, X. Li, and Y. Jian, "Prediction of initial stress of brittle rock expansion-Taking granite and diorite as examples," *Rock mechanics and engineering*, vol. 33, no. 4, pp. 737–746, 2014.
- [30] X. J. Tan, W. Chen, J. Yang, and J. Cao, "Laboratory investigations on the mechanical properties degradation of granite under freeze-thaw cycles," *Cold Regions Science and Technology*, vol. 68, no. 3, pp. 130–138, 2011.
- [31] B. Abernethy and I. D. Rutherford, "The effect of riparian tree roots on the mass-stability of riverbanks," *Earth Surface Processes and Landforms*, vol. 25, no. 9, pp. 921–937, 2000.
- [32] W. Liu, X. Zhang, H. R. Li, and J. Chen, "Investigation on the deformation and strength characteristics of rock salt under different confining pressures," *Geotechnical & Geological Engineering*, vol. 38, no. 6, pp. 5703–5717, 2020.